Structure
Article

Transient Protein States in Designing Inhibitors of the MDM2-p53 Interaction

Michal Bista,[1] Siglinde Wolf,[1] Kareem Khoury,[2,3] Kaja Kowalska,[1] Yijun Huang,[2,3] Ewa Wrona,[6] Marcelino Arciniega,[1] Grzegorz M. Popowicz,[1,5] Tad A. Holak,[1,6,*] and Alexander Dömling[2,3,4,*]
[1]Max-Planck-Institute of Biochemistry, 82152 Martinsried, Germany
[2]Department of Pharmaceutical Sciences, University of Pittsburgh, Biomedical Science Tower 3, 3501 Fifth Avenue, Pittsburgh, PA 15261, USA
[3]Department of Chemistry, University of Pittsburgh, Biomedical Science Tower 3, 3501 Fifth Avenue, Pittsburgh, PA 15261, USA
[4]Department of Drug Design, University of Groningen, A. Deusinglaan 9, 9713 Groningen, the Netherlands
[5]Institute of Structural Biology, Helmholtz Zentrum München, Ingolstädter Landstrasse 1, 85764 Neuherberg, Germany
[6]Organic Chemistry, Jagiellonian University, Ingardena 3, 30-060 Cracow, Poland
*Correspondence: holak@biochem.mpg.de (T.A.H.), a.a.s.domling@rug.nl (A.D.)
http://dx.doi.org/10.1016/j.str.2013.09.006

SUMMARY

Reactivation of p53 by release of the functional protein from its inhibition by MDM2 provides an efficient, nongenotoxic approach to a wide variety of cancers. We present the cocrystal structures of two complexes of MDM2 with inhibitors based on 6-chloroindole scaffolds. Both molecules bound to a distinct conformational state of MDM2 with nM-μM affinities. In contrast to other structurally characterized antagonists, which mimic three amino acids of p53 (Phe19, Trp23, and Leu26), the compounds induced an additional hydrophobic pocket on the MDM2 surface and unveiled a four-point binding mode. The enlarged interaction interface of the inhibitors resulted in extension of small molecules binding toward the "lid" segment of MDM2 (residues 19–23)—a nascent element that interferes with p53 binding. As supported by protein engineering and molecular dynamics studies, employing these unstable elements of MDM2 provides an efficient and yet unexplored alternative in development of MDM2-p53 association inhibitors.

INTRODUCTION

Tumor development requires breaching the line of defense formed by the "guardian of the genome," the tumor suppressor p53 protein (Brown et al., 2009; Cheok, et al., 2011). About 50% of all human cancers inactivate p53 by mutations, and in the remaining the wild-type (WT)-p53 activity is most commonly repressed by the MDM2-mediated ubiquitination (Brown et al., 2009). The release of the functional p53 from its MDM2-mediated regulation provides an efficient, nongenotoxic approach to cancer therapy. Substantial progress has been made in discovering p53-activating molecules in recent years (Cheok et al., 2011; Ding et al., 2013; Vogel et al., 2012; Wade et al., 2013; Zhao et al., 2013). Three different classes of small-molecule MDM2 antagonists are currently under clinical investigation (Wade et al., 2013) and, in addition, p53-stapled peptides have emerged as a promising modality for the p53-Mdm2 and p53-Mdmx interactions (Baek et al., 2012; Chang et al., 2013).

Interaction between p53 and MDM2 involves their N-terminal segments and relies on steric complementarity between the hydrophobic cleft in the p53-binding domain of MDM2 (residues 25–110) and the hydrophobic face of an α helix in the p53 transactivation domain (residues 18–26) (Joerger and Fersht, 2008; Kussie et al., 1996; Popowicz et al., 2011; Stoll et al., 2001). Key to this interaction is a triad of p53 amino acids that insert deeply into the MDM2 cleft: Phe19, Trp23, and Leu26 (designated as three subpockets on MDM2; Figure 1; Figure S1 available online). The MDM2-p53 recognition is a dynamic and multistage process that employs the binding-induced folding of p53 (Kussie et al., 1996; Popowicz et al., 2011; Uesugi and Verdine, 1999; Lee et al., 2000), the rearrangement of the Leu26 subpocket of MDM2 by a twist of the Tyr100 ring from the "closed" to the "open" (anti)conformations (as defined by Popowicz et al., 2007, 2008; Kussie et al., 1996; Dastidar et al., 2009; Uhrinova et al., 2005), and the dissociation of a transient α-helical N-terminal "lid" segment of MDM2 (residues 19–23) from the proximity of the p53-complementary interface (McCoy et al., 2003; Showalter et al., 2008; Zhan et al., 2012).

Until now, all structurally characterized low-molecular-weight inhibitors of the MDM2-p53 interaction targeted the same "closed" Tyr100 state and were incapable of reaching the N-terminal "lid" segment, an intrinsically disordered region of MDM2 (Popowicz et al., 2011; Shangary and Wang, 2009; Dömling, 2008; Graves et al., 2012). Here, we present X-ray structures as evidence of two MDM2 complexes that reveal inhibitor molecules bound to the "open" Tyr100 conformation, leading to a four-point pharmacophore model for this pharmacologically important protein-protein interaction.

RESULTS AND DISCUSSION

Structure of the MDM2-KK271 Complex

Our approach for protein-protein inhibitor development has been based on multicomponent reaction chemistry (Dömling, 2006,

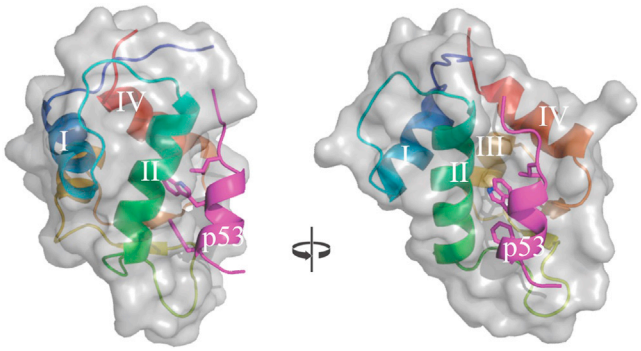

Figure 1. X-Ray Structure of MDM2-p53 Complex
(PDB ID code 1YCR) Numbering of secondary structure elements follows the labels used by Kussie et al. (1996). Because the p53-peptide replaces the N-terminal segment of MDM2, the "lid" helix is dissociated from the surface of MDM2, unfolds, and is invisible in the electron density.
See also Figure S1.

Dömling et al., 2012) (Figure 2) and started with the model that consisted of three features (Popowicz et al., 2011; Shangary and Wang, 2009; Dömling, 2008; Graves et al., 2012) obtained by replacing the key p53 residues by general requirements of hydrophobicity (for Leu and Phe) and adding a specific "anchor" feature constraining the position of a tryptophan analog during the search (Koes et al., 2012; Czarna et al., 2010). This three-point pharmacophore screening yielded compound KK271, which was found to inhibit the MDM2-p53 interaction with K_i = 1,200 nM (Tables 1 and S1). Crystals of the KK271-MDM2 complex unexpectedly revealed two inhibitor molecules bound to a single protein chain (Figures 3 and S2; Table 1). The overall fold of MDM2 in complex with KK271 was similar to the native MDM2-p53 structure with the main-chain root-mean-square deviation (rmsd) of 0.69 Å. The Trp23 pocket of MDM2 is filled with the 6-chloroindole-2-hydroxamic acid, similarly to the native Trp23 of p53, forming extensive hydrophobic interactions with Val93, Gly58, and Leu54. The central, peptidic core of the compound was solvent exposed and did not directly contact the protein, providing the possibility for modifications to improve the drug likeness. Unexpectedly, we found that the isobutyl element filled the Phe19 pocket, and the benzyl moiety was bound within the Leu26 pocket in spite of structural resemblance between the benzyl and isobutyl substituents of KK271 to the p53 amino acids Phe19 and Leu26, respectively. This represents a mirror image of the native p53 interaction with the indole moiety as a pseudoplane of symmetry and is similar to an arrangement previously described for a spiro-oxindole inhibitor (Popowicz, et al., 2010). The isobutyl side chain loosely occupied the Phe19 pocket, forming hydrophobic contacts to Ile61, Val93, and

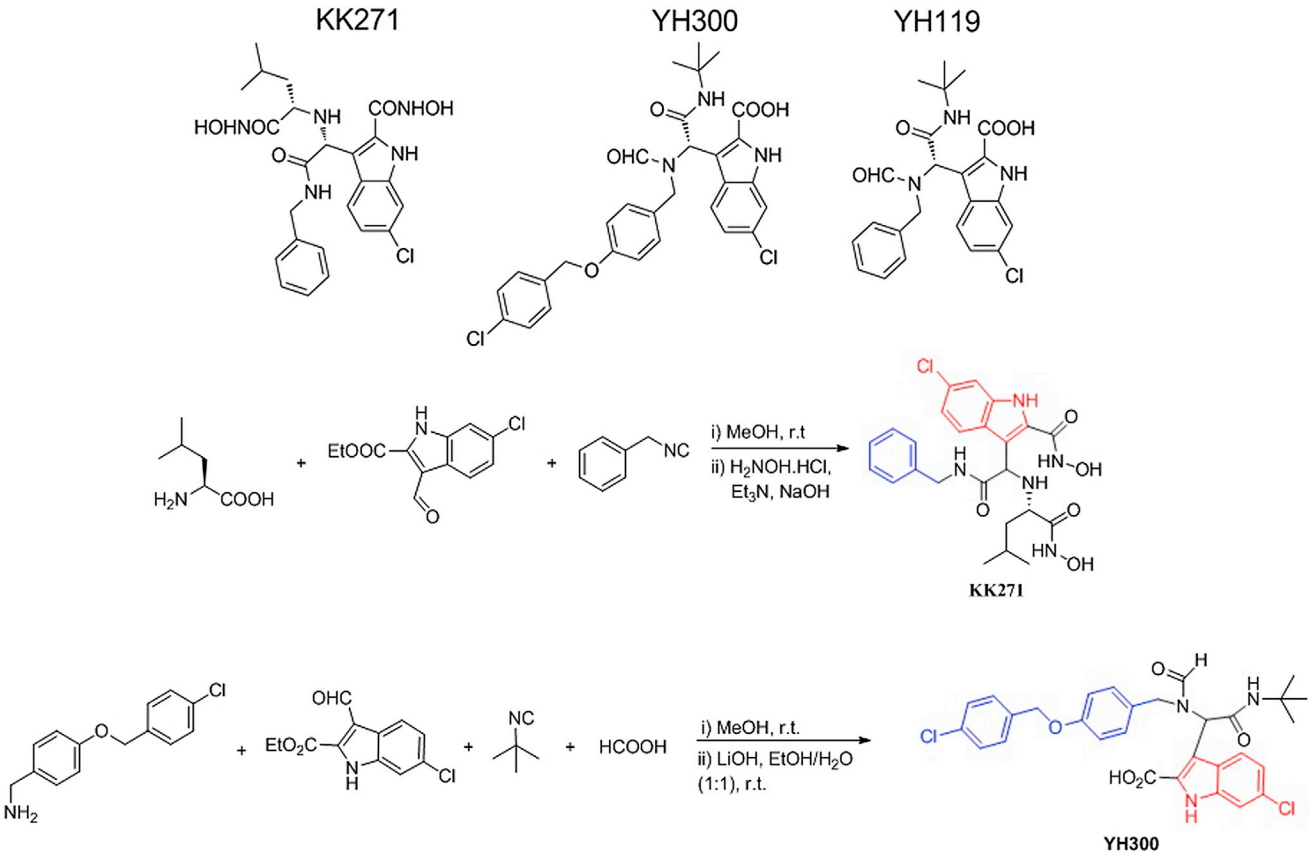

Figure 2. Formulas of Inhibitors and Syntheses of KK271 and YH300
Syntheses of KK271 and YH300 using the one-pot Ugi multicomponent reactions. YH119 was synthesized as described in Huang et al. (2012). The anchoring of the Trp23-mimicking substituent is marked in red, and the Leu25-mimicking moiety is marked in blue.

Table 1. Data Collection and Refinement of Crystallographic Structures and FP Assay Data

	KK271-MDM2	YH300-MDM2
K_i from FP assay (μM)	1.2	0.6
Space group	P 65 2 2	P41 212
Cell constant		
a	53.52	64.341
b	53.52	64.341
c	122.27	81.685
Resolution range (Å)	46.35–2.14	50.54–1.91
Observed reflections	63,031	116,285
Unique reflections	11,501	12,100
Whole resolution range		
Completeness (%)	97.6	94.7
Rmerge (%)	2.6	3.4
I/σ (I)	32.03	26.06
Last resolution shell		
Resolution range (Å)	2.24–2.14	2.0–1.9
Completeness (%)	84.2	97.5
Rmerge (%)	10.0	31.4
I/σ (I)	9.8	4.6
Refinement		
No. of reflections	10,366	13,246
Resolution (Å)	18.5–2.14	20–1.9
R factor (%)	18.5	18.02
Rfree (%)	22.1	20.3
Average B (Å2)	33.3	28.4
Rms bond length (Å)	0.01	0.01
Rms angles (°)	1.8	1.5
Content of asymmetric unit		
No. of complexes	1	1
No. of protein residues/atoms	85/701	94/774
No. of solvent atoms	105	110

See also Figures S2 and S4.

Gly58. Binding of the benzyl group to the Leu26 pocket was substantially different from that of the majority of known inhibitors (Figure S3). Owing to the length and flexibility of the scaffold, this part of the inhibitor binds close to helix IV of MDM2 (Figures 1, 3, and S2) and was involved in a parallel aromatic stacking with His96, with 3.7 Å spacing between the rings. Similar π-stacking contacts were observed in a spirocyclic indolone, α-aminoacylamide (Popowicz, et al., 2010), and chromenotriazolopyrimidine (Allen et al., 2009), but not in the structures of an imidazoline, nutlin, and benzodiazepinedione (Popowicz, et al., 2011, Vassilev et al., 2004; Huang et al., 2012).

Although the binding mode of the first inhibitor was similar to other known antagonists, the presence of the second inhibitor molecule was a surprise. Strikingly, the benzyl group of the second inhibitor molecule is deeply inserted inside MDM2 occupying a double-sized Leu26 subpocket enlarged by rearrangement of Tyr100 side chain into the "open" conformation ($\chi_1 = -171°$). Rearrangement of the Tyr100 ring constrained Tyr104 ($\chi_1 = -131°$) in a conformation with its aromatic plane parallel to the Tyr100 ring plane. The conformational selection of the additional inhibitor molecule was accomplished by flipping the Leu54 side chain to the anticonformation ($\chi_1 = -160°$), maximizing van der Waals contacts with both small molecules.

Structure of the MDM2-YH300 Complex

To test the hypothesis of a general four-point pharmacophore model in the MDM2 receptor, we designed small molecules providing the three-point canonical pharmacophore model and an additional hydrophobic point extending the Leu26-mimicking pharmacophore. Based on the two small molecules binding in the MDM2-KK271 complex, we combined the benzyl group of the first molecule with the phenyl group of the second molecule using a short oxymethylene linker. With this design we hoped to fill the extended Leu26 pocket and to constrain Tyr100 in a position beneficial for binding larger inhibitors. In fact this process yielded, among others, compound YH300 with K_i = 600 nM (Tables 1 and S1). YH300 is an "elongated" derivative of YH119 (Figure 1) previously described by us to have Ki = 1,800 nM (Huang et al., 2012). The cocrystal structure of the MDM2-YH300 complex confirmed that the compound exhibited a four-point interaction mode (Figures 4 and S4). Despite different crystal contacts, both protein chains had very similar structures (with all atom rmsd = 0.07 Å).

As hypothesized, the large 4-chlorobenzyl phenyl ether was found to fill the enlarged Leu26 new subpocket. The pocket is partially formed by the intrinsically disordered N terminus (MQIPASEQV). Moreover, the group forms an extended network of van der Waals contacts with Val93, Leu54, His96, and the Tyr100 in the "open" conformation. The aryl-imidazole π-stacking interaction with His96 is not seen any more in the X-ray lattice because of the shift of the midphenyl ring by ca. 2.3 Å toward the center of the pocket. The His96 side chain does, however, keep electrostatic contacts with the internal aryl group and the methyleneoxy linker fragment. The position of the terminal, 4-chlorophenyl ring overlaps with the phenyl ring of the second KK271 molecule. The Phe19 subpocket is occupied by a tert-butyl group and makes van der Waals contacts with Ile61 and Val93 (analogous to those maintained by KK271).

Molecular Dynamics

The scale of the conformational rearrangements in the protein is clearly visible after removing the inhibitor from the model (Figures 3B and S3). The MDM2 cleft reaches far toward helix IV and is much larger than in other MDM2 complexes. Consequently, the MDM2-KK271 structure represents the most profound example of conformational adaptability of the protein to large ligands. The χ_1 angles of His96 and Tyr100 were observed as indicators of the Leu26 pocket shape (Figures 5, S5, and S6). Interestingly, only the p53-MDM2 complex maintained a stable conformation of these residues (Tyr100 $\chi_1 \approx -120°$, His96 $\chi_1 \approx -60°$) (Figure S6). In the unliganded protein, as well as the KK271 and nutlin-complexes, the side chains of both residues were flipping between two metastable positions: "open" (Tyr100 $\chi_1 \approx -180°$) and "closed" (Tyr100 $\chi_1 \approx -60°$) (Figures 5 and S5). We have also analyzed if the N-terminal fragment of MDM2 has an influence on the behavior of the pocket by

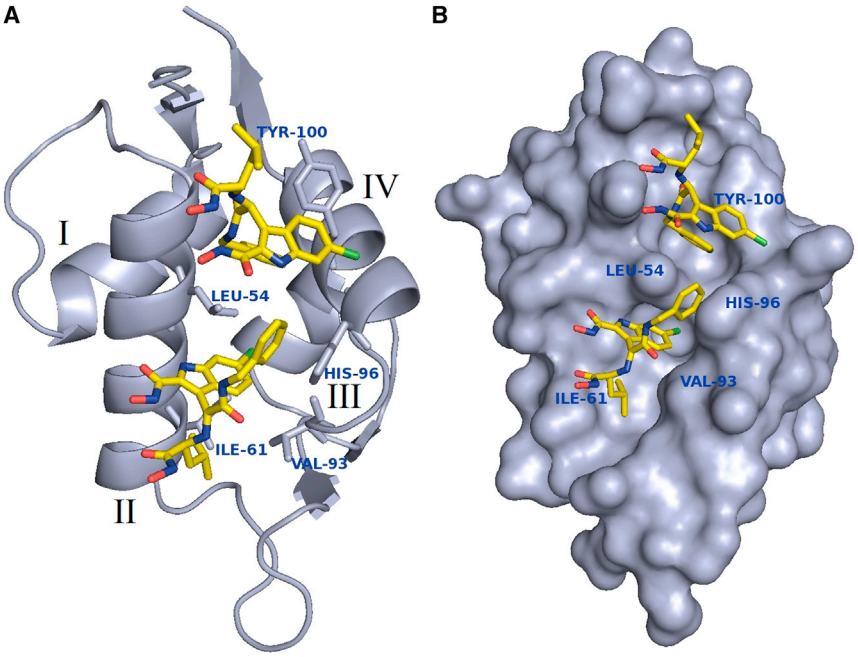

Figure 3. Crystal Structure of KK271 in Complex with MDM2

(A) Key residues of MDM2 in proximity of the two inhibitor molecules are highlighted.

(B) The extended Leu26 pocket is filled with benzyl rings of two inhibitor molecules.

See also Figures S2 and S3.

performing similar simulations on the complexes with an added N-terminal region. The result was similar, revealing additional stabilization of His96 by the N termini (Figure S6) and Tyr100 switching between the "open" and "closed" conformations. The ease of Tyr100 rotation at room temperature and the fact that the "open" conformation was populated for a significant fraction of simulations time, implies that a low-energy barrier of Tyr100 side chain rotation and low difference in the Gibbs free energies exist for the "open" and "closed" Tyr100 rotamers. The previous computational studies performed on MDM2-peptide complexes revealed that both "open" and "closed" Tyr100 states can yield similar binding affinities (Dastidar et al., 2008).

Molecular dynamics simulations performed on the MDM2-YH300 complex confirmed that the four-point binding mode of the inhibitor was preserved and the Tyr100 side chain was stabilized in a single "open" conformation (χ_1 angle $\approx -171°$) (Figure 5) simultaneously forming hydrophobic contacts with the ligand molecule.

NMR Measurements

In the MDM2-YH300 structure, the extended ligand chlorophenyl ring of the inhibitor was buried in a hydrophobic cleft covered by the N-terminal "lid" segment of MDM2 (residues 18–24), and this prompted us to investigate the role of this element in the small-molecule inhibitor binding. It is assumed that at room temperature MDM2 exists in two states: with the "lid" bound (90%) and dissociated (10%) (Showalter et al., 2008), giving ca. 1.2 kcal/mol free energy of dissociation. In order to dissect the role of this element in ligands binding, a mutant MDM2 with the helix-breaking amino acids in the middle of the "lid" element was engineered (the Ser22Pro, Glu23Gly double mutation). Structural properties of the mutant protein were assessed by the ^{1}H-^{15}N-HSQC nuclear magnetic resonance (NMR) spectroscopy. The spectrum of the mutated protein turned out to be significantly different from its wild-type counterpart and not only local but also long-range chemical shift perturbations were observed (Figures 6A and 6B). The two regions most affected by the mutations were the "lid" helix itself and a complementary area proximal to the p53-binding pocket. We found that the pattern of chemical shift perturbations induced by the mutations was in remarkably good agreement with crystallographic structures of MDM2 complexes with the "lid" helix defined by electron density (Figure 6D), proving that despite the dynamic character of the association and crystal lattice packing effects, the static representation provided by our X-ray structures is consistent with the ensemble average in solution state. Furthermore, superposition of the MDM2 X-ray structures containing the "lid" element indicates that it is structurally preserved also in other MDM2 complexes resolved by X-ray crystallography (Figure 6C).

ITC Measurements

To quantify the effect of the "lid" helix on binding of p53, we performed isothermal titration calorimetry with the p53 peptide (residues 19–37) and found that the Ser22Pro Glu23Gly mutations in Mdm2 enhance the affinity of p53 3.3-fold (0.6 kcal/mol difference in the free energies of binding; Tables 2 and S2). Breaking of the "lid" also changed the thermodynamic signature of the interaction by inverting the sign of entropic contribution and making the association enthalpy driven. These differences in the thermodynamics of p53 association with the native and mutant MDM2's may be intuitively explained by competition of the p53 transactivation domain with the transiently structured "lid" that unfolds when not bound (Showalter et al., 2008; Zhan et al., 2012). Finally, we probed the influence of the "lid" element on binding of small molecules. By using a competitive AIDA-NMR experiment (Bista et al., 2009; Czarna et al., 2009; Krajewski et al., 2007), we found that both YH300 and nutlin-3 are less effective in dissociating the mutant-MDM2-p53 complex, owing to a stronger interaction in comparison to the WT-MDM2-p53 interaction (Table S3).

Conclusions

In conclusion, the X-ray structures of the two small-molecule/MDM2 complexes show the inhibitor molecules to be bound to the "open" Tyr100 conformation in a highly extended manner. By developing a line of inhibitors that disrupt the MDM2-p53

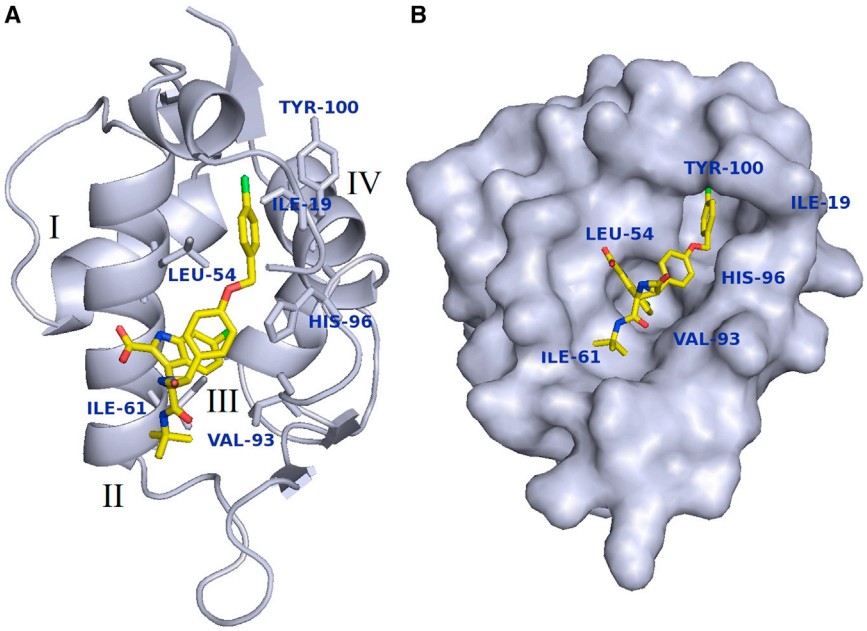

Figure 4. Crystal Structure of YH300 in Complex with MDM2

(A) Key residues of MDM2 around the inhibitor are highlighted.

(B) The 4-chlorobenzyl phenyl ether fills the hydrophobic cavity formed by an extended L26 pocket and the hydrophobic surface of the N-terminal "lid" helix.

See also Figure S4 and Movie S1.

interaction, we demonstrated that rearrangements of aromatic side chains around the p53-interaction interface are associated with only modest energetic penalties (Chen and Luo, 2007; Espinoza-Fonseca and Trujillo-Ferrara, 2006; Espinoza-Fonseca and García-Machorro, 2008) and local instabilities in the protein's binding pocket might be successfully used for extending ligand-protein interaction by formation of a deep hydrophobic pocket formed by back folding of the intrinsically disordered N-terminal lid region, normally seen unfolded in all other MDM2 structures (Movie S1). Therefore, we propose a four-point pharmacophore model that should lead to the design of novel classes of antagonists of the MDM2-p53 interaction and suggest a new possibility of affinity optimization by preventing "lid" dissociation.

EXPERIMENTAL PROCEDURES

Protein Expression, Purification, and Crystallization

Human MDM2 (residues 18–111 or 1–125) was cloned into the pET26 vector and expressed in the *Escherichia coli* BL21(DE3) Rosetta strain (Invitrogen). Cells were grown at 37°C and induced with 1 mM isopropyl β-D-1-thiogalactopyranoside at an OD600 nm of 0.8 and grown for an additional 4 hr at 37°C. The recombinant protein was expressed into inclusion bodies. The inclusion bodies were isolated by centrifugation of the bacterial lysate and washed with PBS containing 0.05% Triton X-100, and they were then subsequently solubilized in 6 M GuHCl in 100 mM Tris-HCl (pH 8.0), including 1 mM EDTA and 10 mM β-mercaptoethanol. The protein was then dialyzed against 4 M GuHCl (pH 3.5) and 10 mM β-mercaptoethanol. For renaturation, the protein was diluted (1:100) into 10 mM Tris-HCl (pH 7.0), containing 1 mM EDTA and 10 mM β-mercaptoethanol, by adding the protein in several pulses into the refolding buffer. Refolding was performed overnight at 4°C. Ammonium sulfate was then added to the final concentration of 1.5 M, and after 3 hr the sample was mixed with 10 ml of the butyl sepharose 4 Fast Flow (Pharmacia, FRG). The protein was eluted with 100 mM Tris-HCl (pH 7.2), containing 5 mM β-mercaptoethanol, and was further purified on the HiLoad 16/60 Superdex200 gel filtration (Pharmacia) into the buffer containing 5 mM Tris-HCl (pH 8.0), 50 mM NaCl, and 10 mM β-mercaptoethanol.

Protein Crystallization

Human MDM2 (residues 18–111) preparations in 5 mM Tris-HCl (pH 8.0), 50 mM NaCl, and 10 mM β-mercaptoethanol were mixed with the molar excess of the small molecule inhibitors; the protein complexes were concentrated to about 20 mg/ml (KK271) or 15 mg/ml (YH300) and subjected to the crystallization screening with the sitting drop vapor diffusion method. The crystals of the MDM2-KK271 complex appeared after several days at 4°C in 0.2 M ammonium nitrate and 20% (w/v) PEG 3350, forming hexagonal bipyramides. The crystals of the MDM2-YH300 complex appeared after several days at 4°C in 0.2M dipotassium phosphate and 2.2 M ammonium sulfate, forming hexagonal bipyramides. All crystals were plunge-frozen in liquid nitrogen, with 30% glycerol added to the mother liquor.

Data Collection and Structure Solution

The data sets were collected on the SLS beamline PXII at the Paul Scherrer Institut. The collected data were indexed, integrated, scaled, and merged with XDS and XSCALE (Kabsch, 1993). The MDM2-KK271 crystal belonged to $P6_522$ space group and diffracted to 2.15 Å, whereas the MDM2-YH300 crystal belonged to $P4_1$ space group and diffracted to 2.0 Å. For KK271-MDM2 crystals, one complex containing one protein molecule and two inhibitor molecules was present in the asymmetric unit; for the YH300-MDM2 crystals, two complexes containing one protein and inhibitor molecules were present in the asymmetric unit. Phase problem was solved by molecular replacement using the Molrep program (Vagin and Teplyakov, 1997) from the CCP4 suite (Bailey, 1994). A MDM2 molecule from MDM2-nutlin cocrystal structure (1RV1; Czarna et al., 2009) was used as a search model. The model was then subsequently improved by Arp/Warp (Perrakis et al., 1999) and manually rebuilt by iterative electron density fitting in MIFit program (http://code.google.com/p/mifit/) and refinement with Refmac5 (Murshudov et al., 1997). Ligand molecule and Refmac5 dictionary restraints were created using the dictionary module in MIFit. Water molecules were added by Arp/Warp solvent module. In a model of KK271-MDM2, the electron densities for residues 18–24 and 109–111 were missing, and thus those residues were not included in the model. For the YH270-MDM2 model, only residue 111 was invisible in the electron density. Additionally, several atoms belonging to side chains atoms without clear electron density were omitted in the model. Data collection and refinement statistics are summarized in Table 1.

Molecular Dynamics

The molecular dynamics (MD) simulations were performed using the GROMACS (v. 5.4.3) molecular modeling package (Van Der Spoel et al., 2005). Starting coordinates of the modeled systems were taken from the respective refined crystallographic structures of protein-ligand complexes. When needed, ligand and/or lid residues (N-terminal) coordinates were removed from the original cocrystallized systems in order to assess its dynamics consequences. All systems were simulated using OPLS all-atom force field (Kaminski et al., 2001) in an explicit water solvent scheme (TIP3 water molecule model [Jorgensen et al., 1983], with 0.15 NaCl concentration for charge neutralization) and periodic boundary conditions. The long-range electrostatic interactions were computed using Fast Particle-Mesh Ewald (PME)

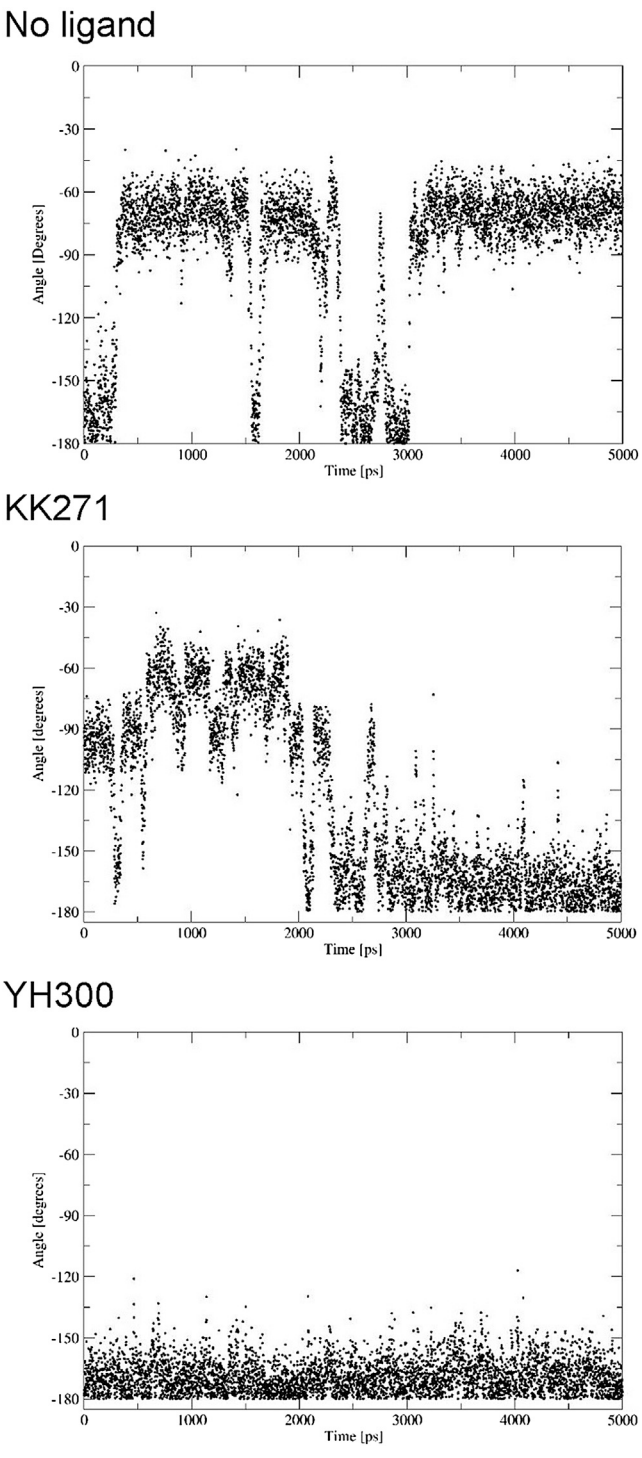

Figure 5. Conformational Dynamics of the Tyr100 Side Chain upon Binding Different Ligands

The Tyr100 side chain is flipping between two metastable "open" and "closed" states. The YH300 molecule is able to stabilize it in "open" conformation.

See also Figures S5 and S6.

(Darden et al., 1993), using a grid spacing of 1.2 Å. The van der Waals and short-range electrostatic interactions were computed using a cutoff of 14 and 11 Å, respectively. The neighbor list was updated every ten steps. The application LINCS algorithm (Hess et al., 1997) to all atom bonds allowed the use of 0.002 ps for time step integration.

An equilibration process was applied to all modeled systems before running the actual production simulation. The equilibration started with two consecutive minimization processes: first, the 2,000 steepest descendant minimization steps, and second, 200 steps using the conjugate gradient algorithm. Subsequently, two short MD simulations (100 ps each) were performed. The first one ran under constant temperature and volume ensemble at 300 K using a Nose-Hoover thermostat (τ = 0.1 ps) (Nose, 1984; Hoover, 1985), followed by second simulation in NTP ensemble using Parrinello-Rahman (Parrinello and Rahman, 1981) pressure coupling at 1 bar (τ = 0.1 ps). Finally, 5 ns of MD simulation in NTP ensemble (keeping the conditions from the last equilibration process) was performed.

Fluorescence Polarization Binding Assays

All fluorescence experiments were performed as described by Czarna et al. (2009). Briefly, the fluorescence polarization experiments were read on an Ultra Evolution 384-well plate reader (Tecan) with the 485 nm excitation and 535 nm emission filters. The fluorescence intensities parallel ($Int_{parallel}$) and perpendicular ($Int_{perpedicular}$) to the plane of excitation were measured in black 384-well NBS assay plates (Corning) at room temperature (~20°C). All fluorescence polarization values were expressed in millipolarization units (mP). The binding affinity of the fluorescent p53-derived peptide of Hu et al. (2007) toward MDM2 protein was determined in a buffer that contained 50 mM NaCl, 10 mM Tris (pH 8.0), 1 mM EDTA, and 10% DMSO. Each sample contained 10 nM of the fluorescent P4 peptide and from 0 to 1 μM of MDM2 in a final volume of 50 μl. Next, the competition binding assays were performed using the 10 nM fluorescent P4 peptide, 15 nM MDM2 (75% of the peptide bound), and ligand concentrations ranging from 0 to 100 μM. Plates were read 30 min after mixing all assay components. Binding constant and inhibition curves were fitted using the SigmaPlot (SPSS Science Software). The experiment results are shown in Table S1.

Isothermal Titration Calorimetry Studies

The isothermal titration calorimetry (ITC) experiments were performed using a Microcal ITC_{200} instrument (Microcal). The sample cell of the calorimeter was loaded with 16 μM MDM2 (1-125) or MDM2 S22P E23G in 50 mM sodium phosphate (pH 7.5), 150 mM NaCl, and 0.5 mM TCEP. The syringe was loaded with chemically synthesized p53 peptide (160 and 140 μM for titrations of wild-type and mutant protein, respectively) in the same buffer. All solutions were degassed for 10 min. Titrations were performed at 20°C with injection volumes of 2 μl and a spacing of 120 s. For the K_D determinations, the baseline was set to zero assuming that the final injections of each titration represent only the heat of dilution. The data were fit using a one-site binding model available in the Origin ITC data analysis software (v. 7.0). The results are shown in Table S2.

NMR Methods

Uniform ^{15}N isotope labeling was achieved by expression of the protein in M9 minimal media containing $^{15}NH_4Cl$ as nitrogen source. All the spectra were recorded at 293 K using Bruker DRX600 spectrometer equipped with a TXI cryoprobe. ^{1}H-^{15}N heteronuclear correlations were obtained using fast HSQC pulse sequence (Mori et al., 1995). Final step of purification of NMR samples was gel filtration into NMR buffer containing 50 mM phosphate (pH 7.2), 150 mM NaCl, and 5 mM DTT. Ten percent (v/v) of D_2O was added to samples to provide lock signal.

Assignment of the amide groups of MDM2 (1-125) was obtained following Stoll et al. (2001) and Showalter et al. (2008). Thanks to relatively good dispersion of MDM2 (1-125), assignment of most of the amide resonances of the mutant MDM2 (1-125 S22P, E23G) was possible by comparison and manual inspection of the spectra. Normalized values of chemical shift perturbations were calculated according to the Pythagoras formula with 15N weighting factor 0.2.

Antagonist-induced dissociation assays (AIDA) (Bista et al., 2009; D'Silva et al., 2005) for investigation of potency of small-molecular weight antagonists to dissociate the MDM2-p53 complex were performed on MDM2(1-125)-p53(1-312) complex using the SEI-AIDA pulse sequence (Bista et al., 2009). For calculation of K_i values of the inhibitors (according to Wang, 1995), K_D of

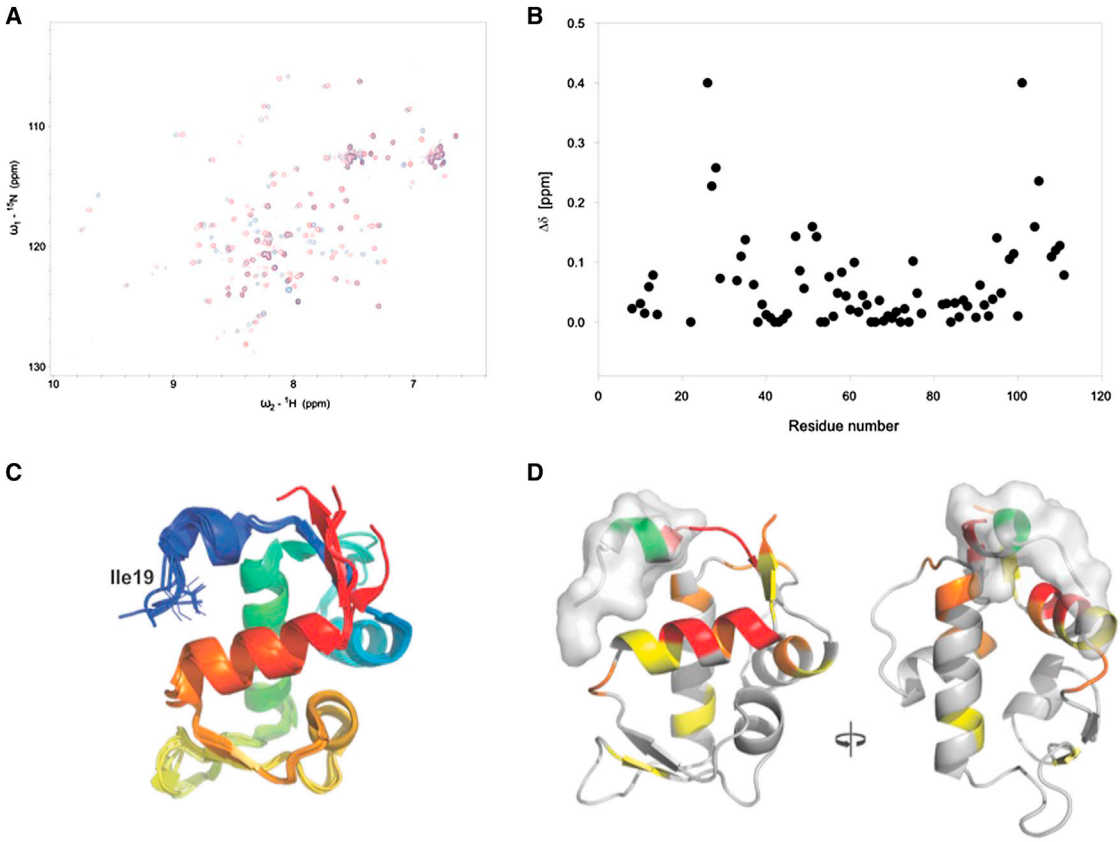

Figure 6. Chemical Shift Mapping of the N-Terminal "Lid" Helix Interaction Site

(A) Overlay of ^{1}H-^{15}N-HSQC spectra of the WT-MDM2 (1–124) (red) and the "lid-broken" mutant Ser22Glue23-Pro22Gly23 (blue).

(B) Normalized chemical shift perturbations as a function of residue number (calculated according to Stoll et al., 2001).

(C) Alignment of X-ray structures of MDM2 demonstrates that conformation and position of the N-terminal "lid" helix are conserved, regardless of crystallization conditions or ligand type. Ile19 side chain covering the extended Leu26 pocket is one of the conserved elements of the N-terminal helix (Macchiarulo et al., 2008).

(D) Chemical shift perturbations plotted onto the structure of MDM2 containing the "lid" element; yellow (>0.075 ppm), orange (>0.1 ppm), and red (>0.125). The "lid" helix is depicted as molecular surface. The site of the mutation is rendered in green. The chemical shifts are concentrated around position of the "lid" seen in crystal structure of MDM2-YH300, confirming that the "lid" in solution maintains similar orientation and interactions.

See also Table S3.

MDM2-p53 interaction was set to the value obtained in ITC measurements with p53 (residues 19–37).

AIDA-NMR Experiment

In this competition experiment (Bista et al., 2009), dissociation of MDM2-p53 complex was monitored by ^{1}H NMR spectroscopy and the MDM2-antagonist inhibition constant was calculated according to Krajewski et al. (2007). Concentrations used in the assay include 6.3 μM MDM2-p53 complex and 6.8 6.3 μM inhibitor. Dissociation constants were assumed to be the same as for the p53 (residues 19–37) peptide used for ITC. Results of the experiment are shown in Table S3.

Table 2. ITC Experiments of Binding p53 Peptide to the Wild-Type and Mutated MDM2

Experiment	Result
MDM2 (1–125) + p53 (17–37)	K_D = 375 (±23) nM ΔH = −7.8 (±0.2) kcal M^{-1} ΔS = 2.7 cal $M^{-1}K^{-1}$
MDM2 (1–125, S22P E23G) + p53 (17–37)	K_D = 112 (±9) nM ΔH = −11.2 (±0.1) kcal M^{-1} ΔS = −6.2 cal $M^{-1}K^{-1}$

See also Table S2.

Synthesis

The compounds were synthetized by two variants of the Ugi multicomponent reactions as depicted in Figure 2. For detail of the syntheses, see the Supplemental Experimental Procedures.

ACCESSION NUMBERS

The coordinates and structure factors have been deposited in the Protein Data Bank with the accession numbers 4MDN and 4MDQ.

SUPPLEMENTAL INFORMATION

Supplemental Information includes Supplemental Experimental Procedures, six figures, three tables, and one movie and can be found with this article online at http://dx.doi.org/10.1016/j.str.2013.09.006.

ACKNOWLEDGMENTS

This research has been supported by grants from the National Institutes of Health (P41 GM094055-02 and 1R01GM097082-01 to A.D.), Marie Curie FP7-Reintegration-Grants within the 7th European Community Framework Programme (to T.A.H.), and a project operated within the Foundation for Polish Science TEAM Programme, cofinanced by the EU European Regional

Development Fund. M.C. was supported by the German Academic Exchange Service (DAAD) (CONACYT-DAAD A/09/72593).

Received: July 26, 2013
Revised: September 10, 2013
Accepted: September 13, 2013
Published: October 24, 2013

REFERENCES

Allen, J.G., Bourbeau, M.P., Wohlhieter, G.E., Bartberger, M.D., Michelsen, K., Hungate, R., Gadwood, R.C., Gaston, R.D., Evans, B., Mann, L.W., et al. (2009). Discovery and optimization of chromenotriazolopyrimidines as potent inhibitors of the mouse double minute 2-tumor protein 53 protein-protein interaction. J. Med. Chem. *52*, 7044–7053.

Baek, S., Kutchukian, P.S., Verdine, G.L., Huber, R., Holak, T.A., Lee, K.W., and Popowicz, G.M. (2012). Structure of the stapled p53 peptide bound to Mdm2. J. Am. Chem. Soc. *134*, 103–106.

Bailey, S.; Collaborative Computational Project, Number 4. (1994). The CCP4 suite: programs for protein crystallography. Acta Crystallogr. D Biol. Crystallogr. *50*, 760–763.

Bista, M., Kowalska, K., Janczyk, W., Dömling, A., and Holak, T.A. (2009). Robust NMR screening for lead compounds using tryptophan-containing proteins. J. Am. Chem. Soc. *131*, 7500–7501.

Brown, C.J., Lain, S., Verma, C.S., Fersht, A.R., and Lane, D.P. (2009). Awakening guardian angels: drugging the p53 pathway. Nat. Rev. Cancer *9*, 862–873.

Chang, Y.S., Graves, B., Guerlavais, V., Tovar, C., Packman, K., To, K.H., Olson, K.A., Kesavan, K., Gangurde, P., Mukherjee, A., et al. (2013). Stapled α-helical peptide drug development: a potent dual inhibitor of MDM2 and MDMX for p53-dependent cancer therapy. Proc. Natl. Acad. Sci. USA *110*, E3445–E3454.

Chen, H.F., and Luo, R. (2007). Binding induced folding in p53-MDM2 complex. J. Am. Chem. Soc. *129*, 2930–2937.

Cheok, C.F., Verma, C.S., Baselga, J., and Lane, D.P. (2011). Translating p53 into the clinic. Nat. Rev. Clin. Oncol. *8*, 25–37.

Czarna, A., Popowicz, G.M., Pecak, A., Wolf, S., Dubin, G., and Holak, T.A. (2009). High affinity interaction of the p53 peptide-analogue with human Mdm2 and Mdmx. Cell Cycle *8*, 1176–1184.

Czarna, A., Beck, B., Srivastava, S., Popowicz, G.M., Wolf, S., Huang, Y.J., Bista, M., Holak, T.A., and Dömling, A. (2010). Robust generation of lead compounds for protein-protein interactions by computational and MCR chemistry: p53/Hdm2 antagonists. Angew. Chem. Int. Ed. Engl. *49*, 5352–5356.

Darden, T., York, D., and Pedersen, L. (1993). Particle mesh Ewald: an N·log(N) method for Ewald sums in large systems. J. Chem. Phys. *98*, 10089–10092.

Dastidar, S.G., Lane, D.P., and Verma, C.S. (2008). Multiple peptide conformations give rise to similar binding affinities: molecular simulations of p53-MDM2. J. Am. Chem. Soc. *130*, 13514–13515.

Dastidar, S.G., Lane, D.P., and Verma, C.S. (2009). Modulation of p53 binding to MDM2: computational studies reveal important roles of Tyr100. BMC Bioinformatics *10*(*Suppl 15*), S6.

Ding, Q.J., Zhang, Z.M., Liu, J.J., Jiang, N., Zhang, J., Ross, T.M., Chu, X.J., Bartkovitz, D., Podlaski, F., Janson, C., et al. (2013). Discovery of RG7388, a potent and selective p53-MDM2 inhibitor in clinical development. J. Med. Chem. *56*, 5979–5983.

Dömling, A. (2006). Recent developments in isocyanide based multicomponent reactions in applied chemistry. Chem. Rev. *106*, 17–89.

Dömling, A. (2008). Small molecular weight protein-protein interaction antagonists: an insurmountable challenge? Curr. Opin. Chem. Biol. *12*, 281–291.

Dömling, A., Wang, W., and Wang, K. (2012). Chemistry and biology of multicomponent reactions. Chem. Rev. *112*, 3083–3135.

D'Silva, L., Ozdowy, P., Krajewski, M., Rothweiler, U., Singh, M., and Holak, T.A. (2005). Monitoring the effects of antagonists on protein-protein interactions with NMR spectroscopy. J. Am. Chem. Soc. *127*, 13220–13226.

Espinoza-Fonseca, L.M., and Trujillo-Ferrara, J.G. (2006). Conformational changes of the p53-binding cleft of MDM2 revealed by molecular dynamics simulations. Biopolymers *83*, 365–373.

Espinoza-Fonseca, L.M., and García-Machorro, J. (2008). Aromatic-aromatic interactions in the formation of the MDM2-p53 complex. Biochem. Biophys. Res. Commun. *370*, 547–551.

Graves, B., Thompson, T., Xia, M., Janson, C., Lukacs, C., Deo, D., Di Lello, P., Fry, D., Garvie, C., Huang, K.S., et al. (2012). Activation of the p53 pathway by small-molecule-induced MDM2 and MDMX dimerization. Proc. Natl. Acad. Sci. USA *109*, 11788–11793.

Hess, B., Bekker, H., Berendsen, H.J.C., and Fraaije, J.G.E.M. (1997). LINCS: a linear constraint solver for molecular simulations. J. Comput. Chem. *18*, 1463–1472.

Hoover, W.G. (1985). Canonical dynamics: equilibrium phase-space distributions. Phys. Rev. A *31*, 1695–1697.

Hu, B., Gilkes, D.M., and Chen, J. (2007). Efficient p53 activation and apoptosis by simultaneous disruption of binding to MDM2 and MDMX. Cancer Res. *67*, 8810–8817.

Huang, Y., Wolf, S., Koes, D., Popowicz, G.M., Camacho, C.J., Holak, T.A., and Dömling, A. (2012). Exhaustive fluorine scanning toward potent p53-Mdm2 antagonists. ChemMedChem *7*, 49–52.

Joerger, A.C., and Fersht, A.R. (2008). Structural biology of the tumor suppressor p53. Annu. Rev. Biochem. *77*, 557–582.

Jorgensen, W.L., Chandrasekhar, J., Madura, J.D., Impey, R.W., and Klein, M.L. (1983). Comparison of simple potential functions for simulating liquid water. J. Chem. Phys. *79*, 926–935.

Kabsch, W. (1993). Automatic processing of rotation diffraction data from crystals of initially unknown symmetry and cell constants. J. Appl. Cryst. *26*, 795–800.

Kaminski, G.A., Friesner, R.A., Tirado-Rives, J., and Jorgensen, W.L. (2001). Evaluation and reparametrization of the OPLS-AA force field for proteins via comparison with accurate quantum chemical calculations on peptides. J. Phys. Chem. B *105*, 6474–6487.

Koes, D., Khoury, K., Huang, Y., Wang, W., Bista, M., Popowicz, G.M., Wolf, S., Holak, T.A., Dömling, A., and Camacho, C.J. (2012). Enabling large-scale design, synthesis and validation of small molecule protein-protein antagonists. PLoS ONE *7*, e32839.

Krajewski, M., Rothweiler, U., D'Silva, L., Majumdar, S., Klein, C., and Holak, T.A. (2007). An NMR-based antagonist induced dissociation assay for targeting the ligand-protein and protein-protein interactions in competition binding experiments. J. Med. Chem. *50*, 4382–4387.

Kussie, P.H., Gorina, S., Marechal, V., Elenbaas, B., Moreau, J., Levine, A.J., and Pavletich, N.P. (1996). Structure of the MDM2 oncoprotein bound to the p53 tumor suppressor transactivation domain. Science *274*, 948–953.

Lee, H., Mok, K.H., Muhandiram, R., Park, K.H., Suk, J.E., Kim, D.H., Chang, J., Sung, Y.C., Choi, K.Y., and Han, K.H. (2000). Local structural elements in the mostly unstructured transcriptional activation domain of human p53. J. Biol. Chem. *275*, 29426–29432.

Macchiarulo, A., Giacchè, N., Carotti, A., Baroni, M., Cruciani, G., and Pellicciari, R. (2008). Targeting the conformational transitions of MDM2 and MDMX: insights into dissimilarities and similarities of p53 recognition. J. Chem. Inf. Model. *48*, 1999–2009.

McCoy, M.A., Gesell, J.J., Senior, M.M., and Wyss, D.F. (2003). Flexible lid to the p53-binding domain of human Mdm2: implications for p53 regulation. Proc. Natl. Acad. Sci. USA *100*, 1645–1648.

Mori, S., Abeygunawardana, C., Johnson, M.O., and van Zijl, P.C. (1995). Improved sensitivity of HSQC spectra of exchanging protons at short interscan delays using a new fast HSQC (FHSQC) detection scheme that avoids water saturation. J. Magn. Reson. B. *108*, 94–98.

Murshudov, G.N., Vagin, A.A., and Dodson, E.J. (1997). Refinement of macromolecular structures by the maximum-likelihood method. Acta Crystallogr. D Biol. Crystallogr. *53*, 240–255.

Nose, S. (1984). A unified formulation of the constant temperature molecular dynamics methods. J. Chem. Phys. *81*, 511–519.

Parrinello, M., and Rahman, A. (1981). Polymorphic transitions in single crystals: a new molecular dynamics method. J. Appl. Physiol. *52*, 7182–7190.

Perrakis, A., Morris, R., and Lamzin, V.S. (1999). Automated protein model building combined with iterative structure refinement. Nat. Struct. Biol. *6*, 458–463.

Popowicz, G.M., Czarna, A., Rothweiler, U., Szwagierczak, A., Krajewski, M., Weber, L., and Holak, T.A. (2007). Molecular basis for the inhibition of p53 by Mdmx. Cell Cycle *6*, 2386–2392.

Popowicz, G.M., Czarna, A., and Holak, T.A. (2008). Structure of the human Mdmx protein bound to the p53 tumor suppressor transactivation domain. Cell Cycle *7*, 2441–2443.

Popowicz, G.M., Czarna, A., Wolf, S., Wang, K., Wang, W., Dömling, A., and Holak, T.A. (2010). Structures of low molecular weight inhibitors bound to MDMX and MDM2 reveal new approaches for p53-MDMX/MDM2 antagonist drug discovery. Cell Cycle *9*, 1104–1111.

Popowicz, G.M., Dömling, A., and Holak, T.A. (2011). The structure-based design of Mdm2/Mdmx-p53 inhibitors gets serious. Angew. Chem. Int. Ed. Engl. *50*, 2680–2688.

Shangary, S., and Wang, S. (2009). Small-molecule inhibitors of the MDM2-p53 protein-protein interaction to reactivate p53 function: a novel approach for cancer therapy. Annu. Rev. Pharmacol. Toxicol. *49*, 223–241.

Showalter, S.A., Bruschweiler-Li, L., Johnson, E., Zhang, F., and Bruschweiler, R. (2008). Quantitative lid dynamics of MDM2 reveals differential ligand binding modes of the p53-binding cleft. J. Am. Chem. Soc. *130*, 6472–6478.

Stoll, R., Renner, C., Hansen, S., Palme, S., Klein, C., Belling, A., Zeslawski, W., Kamionka, M., Rehm, T., Mühlhahn, P., et al. (2001). Chalcone derivatives antagonize interactions between the human oncoprotein MDM2 and p53. Biochemistry *40*, 336–344.

Uesugi, M., and Verdine, G.L. (1999). The α-helical FXXPhiPhi motif in p53: TAF interaction and discrimination by MDM2. Proc. Natl. Acad. Sci. USA *96*, 14801–14806.

Uhrinova, S., Uhrin, D., Powers, H., Watt, K., Zheleva, D., Fischer, P., McInnes, C., and Barlow, P.N. (2005). Structure of free MDM2 N-terminal domain reveals conformational adjustments that accompany p53-binding. J. Mol. Biol. *350*, 587–598.

Vagin, A., and Teplyakov, A. (1997). MOLREP: an automated program for molecular replacement. J. Appl. Cryst. *30*, 1022–1025.

Van Der Spoel, D., Lindahl, E., Hess, B., Groenhof, G., Mark, A.E., and Berendsen, H.J. (2005). GROMACS: fast, flexible, and free. J. Comput. Chem. *26*, 1701–1718.

Vogel, S.M., Bauer, M.R., Joerger, A.C., Wilcken, R., Brandt, T., Veprintsev, D.B., Rutherford, T.J., Fersht, A.R., and Boeckler, F.M. (2012). Lithocholic acid is an endogenous inhibitor of MDM4 and MDM2. Proc. Natl. Acad. Sci. USA *109*, 16906–16910.

Wade, M., Li, Y.C., and Wahl, G.M. (2013). MDM2, MDMX and p53 in oncogenesis and cancer therapy. Nat. Rev. Cancer *13*, 83–96.

Wang, Z.X. (1995). An exact mathematical expression for describing competitive binding of two different ligands to a protein molecule. FEBS Lett. *360*, 111–114.

Vassilev, L.T., Vu, B.T., Graves, B., Carvajal, D., Podlaski, F., Filipovic, Z., Kong, N., Kammlott, U., Lukacs, C., Klein, C., et al. (2004). In vivo activation of the p53 pathway by small-molecule antagonists of MDM2. Science *303*, 844–848.

Zhan, C., Varney, K., Yuan, W., Zhao, L., and Lu, W. (2012). Interrogation of MDM2 phosphorylation in p53 activation using native chemical ligation: the functional role of Ser17 phosphorylation in MDM2 reexamined. J. Am. Chem. Soc. *134*, 6855–6864.

Zhao, Y., Liu, L., Sun, W., Lu, J., McEachern, D., Li, X., Yu, S., Bernard, D., Ochsenbein, P., Ferey, V., et al. (2013). Diastereomeric spirooxindoles as highly potent and efficacious MDM2 inhibitors. J. Am. Chem. Soc. *135*, 7223–7234.